

THREE-DIMENSIONAL SIMULATIONS OF TRANSIENT RESPONSE OF PEM FUEL CELLS

Serhat Yesilyurt

Sabanci University, Istanbul, Turkey
syesilyurt@sabanciuniv.edu

ABSTRACT

Transients have utmost importance in the lifetime and performance degradation of PEM fuel cells. Recent studies show that cyclic transients can induce hygro-thermal fatigue. In particular, the amount of water in the membrane varies significantly during transients, and determines the ionic conductivity and the structural properties of the membrane. In this work, we present three-dimensional time-dependent simulations and analysis of the transport in PEM fuel cells. U-sections of anode and cathode serpentine flow channels, anode and cathode gas diffusion layers, and the membrane sandwiched between them are modeled using incompressible Navier-Stokes equations in the gas flow channels, Maxwell-Stefan equations in the channels and gas diffusion layers, advection-diffusion-type equation for water transport in the membrane and Ohm's law for ionic currents in the membrane and electric currents in gas diffusion electrodes. Transient responses to step changes in load, pressure and the relative humidity of the cathode are obtained from simulations, which are conducted by means of a third party finite-element package, COMSOL.

INTRODUCTION

Modeling and analysis of transport of reactants and flow in PEM fuel cells improve our understanding of PEM operation under normal conditions, transients and failure. In particular, membrane electron assembly has mechanical, electrical and transport properties that depend strongly on hydration and temperature which can be computed by transport models. Due to decreasing cost of computation power and memory, 3D transient models of transport in full active area of a single PEM fuel cell with serpentine flow channels are readily available [1,2]. Moreover, in addition to relative success in tackling of the geometric complexity, modeling the physical complexity of PEM fuel cells remains a challenge; especially those related to multi-scale computational modeling of multiphase flow and transport in PEM fuel cells are addressed by Djilali [3].

Water transport in PEM fuel cell membranes consists of two important mechanisms: diffusion and drag. Both mechanisms are well-known and can be modeled in different ways. Springer et al. [4] use a one-dimensional diffusive model, which is based on the activity of water in the membrane, and empirical electro-osmotic drag. Springer model incorporates Fick's Law with a modified diffusion coefficient, and an empirical electro-osmotic drag coefficient, which is a linear function of the water concentration; thus leading to a transport mechanism that is similar to advection-diffusion equation, in which the advection velocity is the ionic currents of the membrane. Springer's governing equations are widely used in modeling of the water transport in the membrane with small variations in the diffusion coefficient, and in the empirical electro-osmotic drag terms. More elaborate water transport models include the use of two-separate diffusion equations for liquid water and hydronium ions by Berg et al. [5], using Maxwell-Stefan equations to model the diffusion of hydronium ions and water molecules in the solid matrix by Baschuk and Li [6].

In Springer model, boundary conditions are Dirichlet-type, and evaluated based on the absorption values at the catalyst-layers. However, due to significant response times that are observed for the membrane's water intake, several authors suggest that Neumann boundary conditions would be more appropriate in the transient analysis [5-7].

Here, we present time-dependent three-dimensional isothermal single-phase model of:

- Water transport in the membrane based on the Springer model subject to Neumann boundary conditions;
- Transport of species in gas channels and gas diffusion layers by Maxwell-Stefan equations;
- Flow in gas channels by Navier-Stokes equations;
- Darcy's flow in anode gas-diffusion layer;
- Conservation of charge in the membrane and gas diffusion layers in a U-section of a PEMFC with serpentine flow fields as shown in Fig. 1.

The model is essentially similar to our previous two-dimensional model [8].

MODEL DESCRIPTION

Transport of species, charge and flow in the U-section of a PEM fuel cell with serpentine flow fields are modeled here. Figure 1 shows the geometry, and Table 1 shows the geometric parameters of the cell-section. The catalyst layers are very thin and averaged on to the membrane-gas-diffusion-layer interfaces.

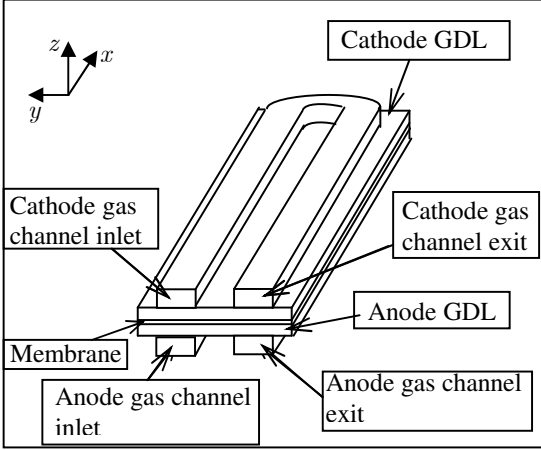


Fig. 1. Outline of the three-dimensional U-section of the PEM fuel cell; the origin of the coordinate system is at the corner of the anode GDL on the exit side.

Table 1. Geometric parameters used in simulations.

Parameter	Value
Flow channel width, δ_{ch}	1 mm
Flow channel height, h_{ch}	0.5 mm
Shoulder separation between flow channels, $\delta_{shoulder}$	1 mm
Gas diffusion layer thickness, δ_{GDL}	0.3 mm
Membrane thickness, δ_m	0.1 mm
Length of the straight part of the channel, ℓ_{ch}	27.5 mm
Extent of the membrane-electrode assembly in the x-direction, ℓ_{MEA}	30 mm
Cathode catalyst layer thickness, $\delta_{cl,ca}$	10 μ m
Anode catalyst layer thickness, $\delta_{cl,an}$	10 μ m

We assume that fuel cell is isothermal and the flow is single phase. Our first assumption relates to relatively small effect of temperature variations within a small section of the fuel cell; and the second assumption is verified with the local activity of water vapor in anode and cathode gas diffusion layers, which does not exceed one.

Governing equations

Transport of gas species

We use Maxwell-Stefan equations to model the transport of gas species in anode and cathode gas diffusion layers and flow channels:

$$\frac{\partial}{\partial t}(\rho \varepsilon_g w_i) + \nabla \left[-\rho w_i \sum_{j=1}^N D_{ij} \left\{ \left(\nabla x_j + (x_j - w_j) \frac{\nabla p}{p} \right) \right\} + \rho w_i \mathbf{u} \right] = 0 \quad (1)$$

where w is the mass fraction and x is the molar fraction of the i^{th} species, i is $\{H_2, H_2O\}$ on the anode side, and $\{O_2, H_2O, N_2\}$ on the cathode side, ε_g is the dry porosity of gas diffusion layers, and is unity in the gas flow channels. In (1), ρ is the density of the mixture, and D_{ij} is the binary diffusion coefficient of species i and j , which is replaced by the effective coefficient, D_{ij}^{eff} , in gas diffusion layers according to a Bruggeman-type relation:

$$D_{ij}^{eff} = D_{ij} \varepsilon_g^{1.5}. \quad (2)$$

Binary diffusion coefficients in mixtures are determined from [10]

$$D_{ij} = 3.16 \times 10^{-8} \left(\frac{T^{1.75}}{p(v_i^3 + v_j^3)^2} \right) \left(\frac{1}{M_i} + \frac{1}{M_j} \right)^{1/2} \quad (3)$$

where, v_i is the molar volume of species i , T is the temperature, and M_i is the molecular weight of species, i . In (1) and (3) p is the total pressure, which is set to anode and cathode inlet pressures respectively.

The flow field

The velocity vector, \mathbf{u} , in (1) is obtained from the molar average velocity in the cathode gas diffusion layer. Since N_2 is the inert gas in the cathode its mass flux is zero and can be used to determine the convective velocity without needing extra degrees of freedom and additional equations. Thus, the velocity field in cathode gas diffusion layers, $\mathbf{u}_{ca,GDL}$, is determined from the N_2 diffusive mass-flux in the cathode gas diffusion layer as follows:

$$\mathbf{u}_{ca,GDL} = \sum_{i=\{O_2, H_2O\}} D_{i-N_2}^{eff} \nabla \left(\frac{w_i}{M_i} \frac{1}{\sum_{j=\{O_2, H_2O, N_2\}} \frac{w_j}{M_j}} \right) \quad (4)$$

In the anode gas diffusion layer we do not have an inert gas to determine the molar average velocity, however we can determine the velocity, $\mathbf{u}_{an,GDL}$, with a single unknown field, *pressure* using Darcy's Law as it is reasonable to model the flow in the gas diffusion layer as the flow in porous medium:

$$\mathbf{u}_{an,GDL} = -\frac{\kappa}{\mu} \nabla p, \quad (5)$$

where, κ , is the permeability, and μ is the viscosity of the mixture. The velocity field in the anode gas diffusion layer is subject to continuity equation:

$$\frac{\partial}{\partial t}(\rho \varepsilon_g) + \nabla \cdot (\rho \varepsilon_g \mathbf{u}_{an,GDL}) = 0. \quad (6)$$

Finally, in flow channels incompressible Navier-Stokes equations are used to compute the velocity:

$$\rho \left(\frac{\partial \mathbf{u}}{\partial t} + \mathbf{u} \cdot \nabla \mathbf{u} \right) = -\nabla p + \mu \nabla^2 \mathbf{u} \quad (7)$$

subject to $\nabla \cdot \mathbf{u} = 0$

where ρ and μ are the density and viscosity of the gas mixtures in anode and cathode flow channels.

Transport of water in the membrane

Transport of liquid water in the membrane is modeled by advection-diffusion equation, where the advection is due to ion currents in the membrane, similar to the Springer model [4] as follows:

$$\frac{\partial}{\partial t}(\varepsilon_m c_w) = -\nabla \cdot \left(-D_w \nabla c_w + \frac{M_m}{\rho_m} \frac{\mathbf{J}_+}{F} \frac{c_w}{n_{d,A}} \right) \quad (8)$$

where ε_m is the membrane porosity, c_w is the number of water molecules per sulfonic group in the membrane, D_w is the diffusion coefficient given by [11], M_m is the membranes molecular weight, ρ_m is membrane's density, F is the Faraday constant, \mathbf{J}_+ is the ionic current vector, and $n_{d,A}$ is a constant which quantifies the electro-osmotic drag of water molecules per each proton, i.e.

$$n_d = \frac{c_w}{n_{d,A}}. \quad (9)$$

Membrane ionic potential

In (8), proton current through the membrane, \mathbf{J}_+ , is given by the Ohm's Law, and subject to conservation of charge, i.e.

$$\nabla \cdot \mathbf{J}_+ = 0, \quad \mathbf{J}_+ = -\sigma_m \nabla \phi_m \quad (10)$$

Here, ϕ_m is the ionic potential, and σ_m is the membrane's ionic conductivity of the membrane given by the empirical formula [4]:

$$\sigma_m = (0.5139c_w - 0.326) \exp \left[1268 \left(\frac{1}{303} - \frac{1}{T} \right) \right]. \quad (11)$$

Electric potential

Similarly in gas diffusion layers, the electric current is given by Ohm's Law and subject to conservation of charge:

$$\nabla \cdot \mathbf{J}_e = 0, \quad \mathbf{J}_e = -\sigma_e \nabla \phi_e, \quad (12)$$

where, σ_e is the electrode's effective conductivity, and ϕ_e is the electric potential.

Boundary conditions

For Maxwell-Stefan equations

Maxwell-Stefan equation governs the mass transport in anode flow channel and in anode gas diffusion layer. Thus, at the channel-gas-diffusion-layer interface, we do not need to specify any conditions as the mass fractions and fluxes of species are automatically continuous. However, the conditions at the channel inlet, outlet and the membrane boundary that corresponds to the catalyst layer must be specified.

At the anode inlet, hydrogen's mass fraction is specified:

$$w_{H_2} = w_{H_2,in}. \quad (13)$$

At the anode exit, normal component of the diffusive mass flux of hydrogen is zero.

$$\mathbf{n} \cdot (-\rho w_{H_2} D_{H_2-H_2O} \nabla x_{H_2O}) = 0. \quad (14)$$

At the anode catalyst layer, which is averaged on to the membrane-anode interface, inward mass flux of hydrogen is specified according to the electrochemical reaction in the catalyst layer specified by the anode exchange current density, i_a :

$$-\mathbf{n} \cdot [\rho w_{H_2} (-D_{H_2-H_2O} \nabla x_{H_2O} + \mathbf{u})] = \frac{M_{H_2} i_a}{2F}. \quad (15)$$

The exchange current density, i_a , at the anode catalyst layer is defined by the Butler-Volmer expression:

$$i_a = S_{an} \delta_{cl,an} i_{0,an} \left(\frac{c_{H_2}}{c_{H_2,ref}} \right)^{1/2} \left(\frac{F}{RT} \right) (\phi_e - \phi_m - \phi_{over,an}), \quad (16)$$

where S_{an} is the active area of the catalyst in units of $[m^2/m^3]$, $\delta_{cl,an}$ is the thickness of the catalyst layer, $i_{0,an}$ is the reference current density, $c_{H_2,ref}$ is the reference hydrogen concentration, and $\phi_{over,an}$ is the anode over potential, which is taken as zero.

At the channel walls, and the rest of the boundaries of the anode gas diffusion layer, the zero total flux boundary conditions are specified.

On the cathode side, boundary conditions of Maxwell-Stefan equations are similar to those on the anode side. Namely, at the interface between the flow channels and the cathode gas diffusion layers mass fractions and fluxes are continuous. At the cathode channel inlet, mass fractions of oxygen and water vapor are specified according to the composition of standard air and specified cathode-inlet relative-humidity:

$$w_{O_2} = w_{O_2,in} \quad \text{and} \quad w_{H_2O} = w_{H_2O,in}. \quad (17)$$

At the cathode exit, normal components of the diffusive fluxes of hydrogen and water vapor are zero:

$$\mathbf{n} \cdot \left(-\rho w_i \sum_{j \neq i} D_{ij} \nabla x_j \right) = 0, \quad i, j = \{O_2, H_2O, N_2\} \quad (18)$$

At the cathode gas-diffusion-layer-membrane interface, inward mass fluxes of oxygen and water are specified according to the electrochemical reaction rate specified by the cathode exchange current density, the electro-osmotic drag and diffusion of water from the membrane. For oxygen, we have:

$$-\mathbf{n} \cdot \left[\rho w_{O_2} \left(-\sum_{j \neq O_2} D_{O_2-j} \nabla x_j + \mathbf{u} \right) \right] = \frac{M_{O_2} i_c}{4F}. \quad (19)$$

Total flux of the water vapor is directly coupled to the water flux coming from the membrane, which is also coupled to the ionic currents:

$$-\mathbf{n} \cdot \left[\rho w_{H_2O} \left(-\sum_{j \neq H_2O} D_{H_2O-j} \nabla x_j + \mathbf{u} \right) \right] = -M_{H_2O} \left[\frac{i_c}{F} \left(\frac{1}{2} + \frac{c_w}{n_{d,A}} \right) - \frac{\rho_m}{M_m} (D_w \nabla c_w) \cdot \mathbf{n} \right] \quad (20)$$

where \mathbf{n} is the normal of the surface (in the direction towards the membrane).

In (19) and (20), the exchange current density at the cathode catalyst layer is given by the Butler-Volmer expression:

$$i_c = S_{ca} \delta_{cl,ca} i_{0,ca} \left(\frac{c_{O_2}}{c_{O_2,ref}} \right) \exp \left(-\frac{F}{RT} (\phi_c - \phi_m - \phi_{over,ca}) \right), \quad (21)$$

where S_{ca} is the active area of the catalyst in units of $[m^2/m^3]$, $\delta_{cl,ca}$ is the thickness of the catalyst layer, $i_{0,ca}$ is the reference current density, $c_{O_2,ref}$ is the reference oxygen concentration, and $\phi_{over,ca}$ is the cathode over potential, which is given by an empirical relation as a function of operation temperature:

$$\phi_{over,ca} = 0.2329 + 0.0025 \times T. \quad (22)$$

For Darcy's Law (anode gas diffusion layer)

Boundary conditions for the pressure in anode gas diffusion layer in (5) and (6) are specified pressure on the anode gas channel side as

$$p = p_{an,in}. \quad (23)$$

On the anode gas-diffusion-layer-membrane interface, total flow due to electrochemical reaction of hydrogen and drag of water is specified as the velocity boundary condition and coupled to the membrane water transport and ionic currents:

$$-\mathbf{n} \cdot \mathbf{u} = \frac{1}{\rho} \left[\frac{i_a}{F} \left(\frac{M_{H_2}}{2} + M_{H_2O} \frac{c_w}{n_{d,A}} \right) - \left(\frac{\rho_m}{M_m} M_{H_2O} \right) \mathbf{n} \cdot (-D_w \nabla c_w) \right]. \quad (24)$$

The rest of the boundary conditions are zero velocity insulation conditions.

For Navier-Stokes equations

The velocity vector in gas channels is calculated from (7) subject to no slip conditions at the channel walls including the gas-diffusion-layer interfaces. At anode and cathode inlets and outlets of the flow channels, pressures are specified as follows:

$$\begin{aligned} \text{Anode inlet: } p &= p_{an,in}, \quad \text{outlet: } p = p_{an,in} - \Delta p_{an} \\ \text{Cathode inlet: } p &= p_{ca,in}, \quad \text{outlet: } p = p_{ca,in} - \Delta p_{ca} \end{aligned} \quad (25)$$

For advection-diffusion equation

Equation (8) governs the water transport in the membrane, and is subject to flux boundary conditions on the anode and cathode sides similar to formulations used in [5,7-9]. On the anode side, the inward flux is specified as:

$$-\mathbf{n} \cdot \left(-D_w \nabla c_w + \frac{M_m}{\rho_m} \frac{c_w}{n_{d,A} F} \mathbf{J}_+ \right) = -h_m^{an} (c_w - c_w^{an,*}) + \frac{i_a}{F} \frac{M_m}{\rho_m}, \quad (26)$$

where, h_m^{an} is the rate constant for Henry's Law on the anode side, and $c_w^{an,*}$ is the equilibrium sorption value of the water activity on the anode side. Similarly on the cathode side, we have

$$-\mathbf{n} \cdot \left(-D_w \nabla c_w + \frac{M_m}{\rho_m} \frac{c_w}{n_{d,A} F} \mathbf{J}_+ \right) = -h_m^{ca} (c_w - c_w^{ca,*}) - \frac{M_m}{\rho_m} \frac{3}{2} \frac{i_c}{F}, \quad (27)$$

where, h_m^{ca} is the cathode-side rate constant for Henry's Law, and $c_w^{ca,*}$ is the cathode-side equilibrium sorption value.

Anode-side and cathode-side rate constants of Henry's Law can be called as mass transfer coefficients [5] as well as humidification parameters [9].

The rest of the boundaries are subject to insulation conditions.

For membrane potential

The ionic potential in the membrane is governed by Equation (10), and subject to specified current boundary conditions on the anode and cathode sides, namely the inward current on the anode side is given by,

$$\text{Anode side: } -\mathbf{n} \cdot \mathbf{J}_+ = -i_a, \quad (28)$$

where the exchange current density, i_a , is given by (16). Similarly, on the cathode side, the inward current is specified as follows:

$$\text{Cathode side: } -\mathbf{n} \cdot \mathbf{J}_+ = -i_c, \quad (29)$$

where the exchange current density, i_c , is given by (21).

Other boundaries are subject to insulation conditions.

For electric potential

The electric potential distribution in the gas diffusion layers is governed by (12), and is subject to ground boundary conditions.

tion on the anode shoulders, which are in contact with a current collecting plate:

$$\text{Anode shoulders: } \phi_e = 0. \quad (30)$$

On the anode-side gas-diffusion-layer-membrane interface, the electric current is specified as the anode exchange current density:

$$\text{Anode-membrane interface: } -\mathbf{n} \cdot \mathbf{J}_e = i_a, \quad (31)$$

Similarly, at the cathode-membrane interface, the electric current into the gas-diffusion layer is specified as the negative of the cathode exchange current density:

$$\text{Cathode-membrane interface: } -\mathbf{n} \cdot \mathbf{J}_e = -i_c. \quad (32)$$

Finally at the cathode shoulder, the cell voltage is specified:

$$\text{Cathode shoulders: } \phi_e = V_{cell}. \quad (33)$$

Other boundaries for the electric potential are set to insulation conditions.

Table 2 shows the transport and electric properties of the membrane, gas diffusion layer and operating conditions used in the model.

Numerical procedure

Equations (1),(6),(7),(8),(10) and (12) subject to boundary conditions (13)-(15), (17)-(20), and (23)-(33) are solved with the commercial software package COMSOL, that utilizes the finite-element method [12]. The mesh is discretized with 8100 second-order tensor-product (“brick”) elements, with 195000 total numbers of degrees of freedom. For transient simulations initial conditions are started from steady-state conditions, and coupled equations are solved altogether. Steady-state simulations do not converge when coupled equations are solved together, for convergence the following solution order converged in many cases.

1. Set initial conditions for mass fractions as inlet mass fractions, anode pressure as anode inlet pressure in anode-side Darcy’s equation, and fully humidified membrane for convection-diffusion equation, i.e. $c_w=14$.
2. Solve for membrane potential and update initial guess for the nonlinear solver using already obtained values.
3. Solve for membrane and electric potential together and update the initial guess.
4. Solve Navier-Stokes and update the initial guess.
5. Solve for membrane and electric potentials, Maxwell-Stefan and Navier-Stokes equations together and update the initial guess.
6. Solve for membrane and electric potentials, Maxwell-Stefan, Navier-Stokes and Darcy’s equations together and update the initial guess.
7. Solve for all equations coupled together.

Once a steady-state solution is obtained, parametric solutions where one of the parameters such as the inlet-outlet pressure difference, relative humidity, cell voltage may be varied slightly and coupled equations may be solved together for the

new value of the selected parameter. Moreover, by specifying a time-variation in the selected parameter, such as a step change at a specified time, time-dependent coupled equations can be solved together for the transient.

Table 2. Material properties and the base operating conditions of the fuel cell section

Property	Value
Fuel cell temperature, T_θ [K]	353
Faraday’s constant, F [C-mol ⁻¹]	96487
Universal gas constant, R [J·kg ⁻¹ mol ⁻¹]	8.31
Molar volume of oxygen, v_{O_2} [m ³ mol ⁻¹]	16.6×10 ⁻⁶
Molar volume of nitrogen, v_{N_2} [m ³ mol ⁻¹]	17.9×10 ⁻⁶
Molar volume of water vapor, v_{H_2O} [m ³ mol ⁻¹]	12.7×10 ⁻⁶
Porosity of the gas diffusion layer, ϵ_g	0.5
Porosity of the membrane, ϵ_m	0.28
Permeability of gas diffusion layers, κ_{GDL} [m ²]	10 ⁻¹³
Active area of the cathode catalyst layer, S_{ca} [m ²]	10 ⁵
Active area of the anode catalyst layer, S_{an} [m ²]	10 ⁵
Anode reference current density, $i_{o,ca}$ [A-m ⁻²]	10 ⁻⁴
Cathode reference current density, $i_{o,ca}$ [A-m ⁻²]	1
Cathode inlet pressure, $p_{ca,in}$ [atm]	2
Anode inlet pressure, $p_{an,in}$ [atm]	2
Anode pressure drop, Δp_{an} [Pa]	30
Cathode pressure drop, Δp_{ca} [Pa] (when unspecified)	500
Hydrogen reference concentration, $c_{H_2,ref}$ [mol-m ⁻³]	40
Oxygen reference concentration, $c_{O_2,ref}$ [mol-m ⁻³]	40
Coefficient of electro-osmotic drag, $n_{d,A}$	22
Cathode gas viscosity, μ_c [Pa-s]	2.08×10 ⁻⁵
Anode gas viscosity, μ_a [Pa-s]	3×10 ⁻⁵
Anode inlet relative humidity, RH_a [%]	100
Electric conductivity of GDL, σ_e [S-m]	100

In both steady-state and transient cases, COMSOL’s PARDISO solver is used along with Intel’s MKL-BLAS library where automatic parallelization is invoked when specified. A typical steady-state simulation that restarts from an existing solution takes about 15 minutes on 4 nodes of a dual quad-core 2.4 GHz Intel-Xeon workstation with 16 GB Ram and running 64-bit SUSE10.2 Linux operating system. A 20-second transient simulation takes about 30 minutes to 2 hours on the same system.

RESULTS AND DISCUSSION

In what follows all transients start at $t = 1$ second, and follows a sharp ramp to its final value within 0.25 seconds. In transient comparisons, area-averaged cell current and volume averaged membrane water content are used. The former is defined as the ratio of the area integral of the electric current over the cathode shoulder divided by the shoulder area:

$$I_{cell,av} = \frac{\int_{Cathode\ shoulder} \mathbf{n} \cdot \mathbf{J}_e dA}{A_{cathode\ shoulder}} \quad (34)$$

Volume-averaged membrane water content is defined as:

$$c_{w,av} = \frac{\int_{Membrane} c_w dV}{V_{membrane}} \quad (35)$$

Electric load transients

In (33), boundary conditions for the electric potential are specified as the cell voltage. Thus electric load conditions vary according to the cell voltage. In Fig. 2, transient responses of area-averaged currents are shown with respect to a transient cell voltage that is lowered to 0.7 Volts from 0.75 Volts for two different cathode humidity conditions, and two different humidification parameters (rate constants of membrane's water absorption according to Henry's Law). In all cases that are shown here, transient response of the cell current exhibits an overshoot behavior. Initial jump in the average current is due to initial drop in the cathode overpotential, followed by a decreasing stoichiometric flow ratio, which is shown in Fig. 3, due to constant pressure drop specified at the cathode channel as $\Delta p_c = 500$ Pa.

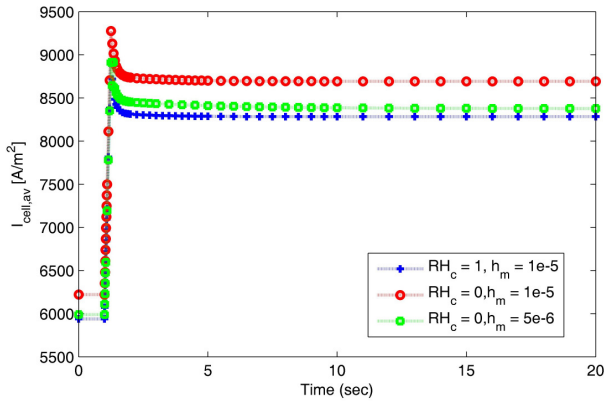


Fig. 2: Area averaged current density at the collectors with respect to time following the decrease of cell voltage from 0.75 to 0.70 linearly in 0.25 seconds at $t=1$ sec.

The effect of cathode humidity in the load transient is shown in the first two plots according to the legend of the graph in Fig. 2. In both plots the humidification factors are the same,

$h_m = 1 \times 10^{-5}$ m/s. Fully humidified cathode inlet leads to a lower steady-state average cell current than dry cathode inlet does; and voltage transients develop accordingly.

The effect of the humidification factor in load transients is observed in the comparison of the last two curves in Fig. 2 according to its legend. In essence, large humidification parameter results in larger cell average current due to larger water content in the membrane and, hence, larger ionic conductivity of the membrane than small humidification parameter does.

In Fig. 4, response of the volume-averaged membrane-water-content is shown. Clearly, larger the cathode inlet humidity, larger the water content in the membrane. Moreover, water content of the membrane is also larger for $h_m = 1 \times 10^{-5}$ m/s than for $h_m = 5 \times 10^{-6}$ m/s. Lastly, it is clear in Fig. 4 that the transient is slower when the humidification factor is smaller.

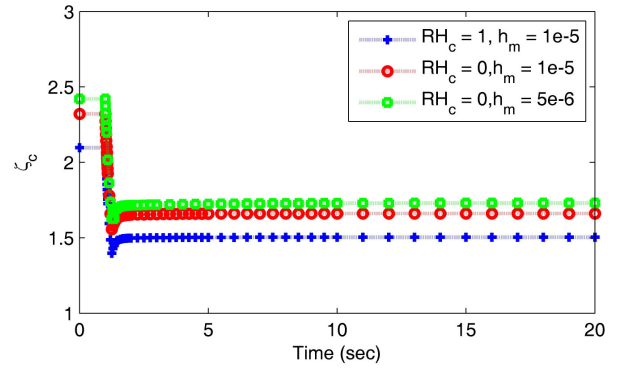


Fig. 3: Cathode stoichiometric flow ratio as a function of time following the decrease of cell voltage from 0.75 to 0.70 linearly in 0.25 seconds at $t=1$ sec.

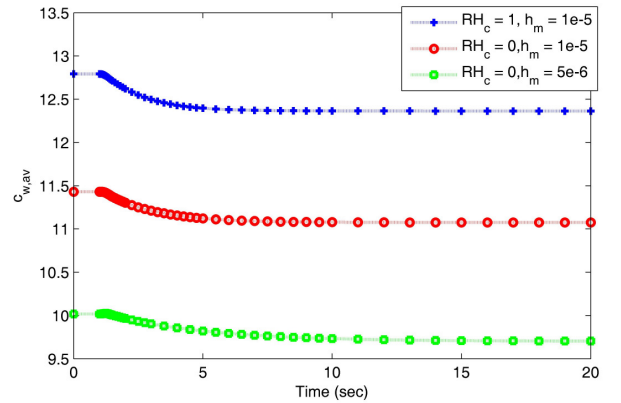


Fig. 4: Volume-averaged membrane-water concentration as a function of time following the decrease of cell voltage from 0.75 to 0.70 linearly in 0.25 seconds at $t=1$ sec.

Effect of the humidification parameter

The application of Neumann boundary conditions in the advection-diffusion equation for the membrane water leads to two time-scales associated with the membrane's water transport: diffusive and humidification time-scales. Standard diffusive

time scale is proportional to the ratio of the square of the membrane's thickness and the diffusion coefficient, that is:

$$\tau_D = \frac{\delta_m^2}{D_{w,av}}. \quad (36)$$

The humidification time-scale can be obtained from the volume-averaging of (8) along with replacing the volume integral of the right-hand-side of (8) by the area integral over the surfaces using the Green's Theorem. Thus, from (26) and (27), neglecting the nonlinear effect of the exchange currents, we have:

$$\frac{dc_{w,av}}{dt} = -(h_m^{ca} + h_m^{an})c_{w,av} + h_m^{ca}c_w^{ca,*} + h_m^{an}c_c^{an,*}. \quad (37)$$

+ nonlinear terms from the reaction

Then, the humidification time-scale can be estimated as:

$$\tau_h \approx \frac{\delta_m}{h_m^{an} + h_m^{ca}}. \quad (38)$$

In fact, the ratio of the two time-scales can be interpreted as a mass transfer Biot number, which is:

$$Bi_m = \frac{\tau_D}{\tau_h} = \frac{(h_m^{an} + h_m^{ca})\delta_m}{D_{w,av}} \quad (39)$$

For the parameters used in simulations, for $h_m^{an} = h_m^{ca} = h_m = 1 \times 10^{-5}$ m/s, we have $\tau_h = 5s$, and for $h_m^{an} = h_m^{ca} = h_m = 5 \times 10^{-6}$ m/s, we have $\tau_h = 10s$. Diffusive time-scales in both cases remain constant, $\tau_D \approx 10^{-8}/4 \times 10^{-8} = 0.25s$, where the diffusion coefficient of water for $c_w \approx 10$ is about 4×10^{-8} according to the water's diffusion coefficient in the membrane.

Neglecting the effect of the nonlinear reaction terms a general solution to (37) is given by:

$$c_{w,av} = c_{w,av}(\infty) + (c_{w,av}(0) - c_{w,av}(\infty))\exp(-t/\tau), \quad (40)$$

In (4), τ is the time-constant, and obtained from the slope of the plot, in which the logarithm of the normalized volume averaged membrane water concentration, $\log[(c_{w,av} - c_{w,av}(\infty))/(c_{w,av}(0) - c_{w,av}(\infty))]$, is plotted against the time after the transient, as shown in Fig. 5.

Humidification time constants for those three conditions are obtained as (see Fig. 5): $\tau_h = 1.5s$ seconds for $RH_c = 1$ and $h_m = 1 \times 10^{-5}$ m/s; $\tau_h = 2s$ seconds for $RH_c = 0$ and $h_m = 1 \times 10^{-5}$ m/s; and $\tau_h = 4s$ seconds for $RH_c = 0$ and $h_m = 5 \times 10^{-6}$ m/s. When the cathode inlet relative humidity is zero, doubling the humidification parameter results in twice as small time-constant in agreement with (38). However, Eq. (38) does not reflect the dependence of anode and cathode equilibrium values, $c_w^{an,*}$ and $c_w^{ca,*}$ on the membrane water concentration. Furthermore neglected reaction terms also have a nonlin-

ear dependence on the membrane water concentration. Thus for the same humidification parameter when conditions vary time-constants also vary, such as when the relative humidity at the cathode inlet increases time-scale also increases as shown in Figs. 4 and 5.

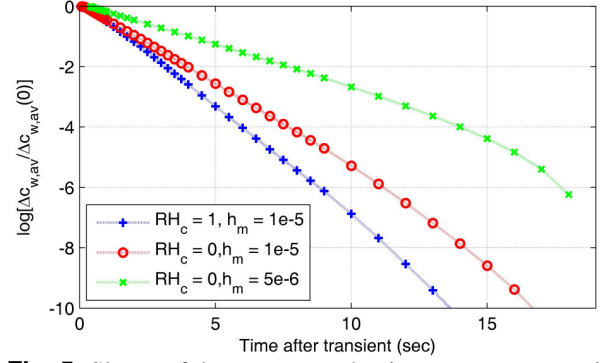


Fig. 5: Slopes of the curves are the time-constants associated with the membrane water concentration transients in Fig. 4.

Cathode humidification transients

Boundary conditions for oxygen and water inlet mass fractions are determined from the specified inlet relative humidity as well as cathode pressure and fuel cell isothermal temperature. Responses are obtained for the average cell current density, in Fig. 6, and membrane water concentration, in Fig. 7, with respect to transients of relative humidity at the cathode inlet.

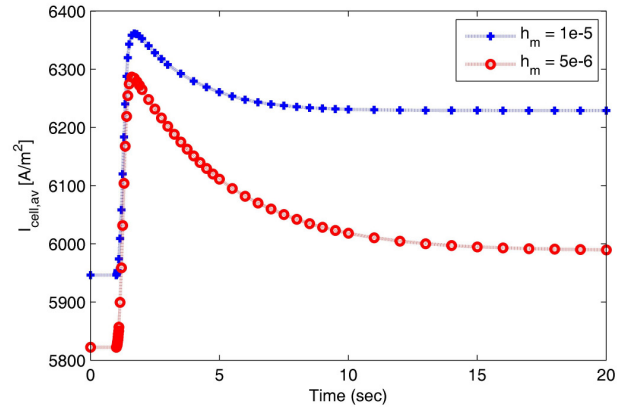


Fig. 6: Area averaged current density at the collectors with respect to time following the decrease of cathode inlet relative humidity from 100% to 0% linearly in 0.25 seconds at $t=1$ sec.

In humidification transients, relative humidity of the cathode is decreased to zero from one at $t = 1$ s linearly with a ramp that lasts 0.25 seconds when the cell voltage is fixed at 0.75 Volts. Current response strongly depends on the humidification parameter: shorter response time and larger currents are observed for large humidification parameter than small one. In both cases, current responses exhibit a slow decaying over-

shoot, and average water concentration transients are simple decays.

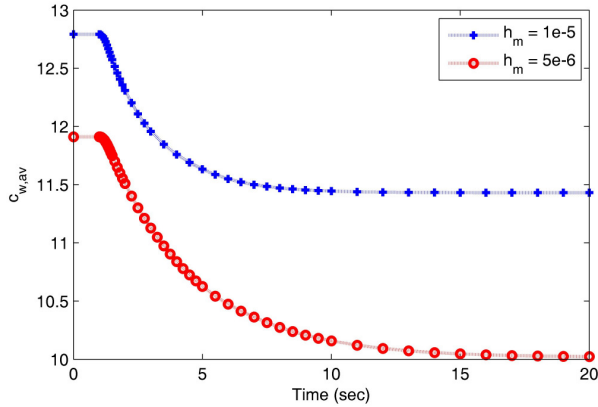


Fig. 7: Volume-averaged membrane-water concentration as a function of time following the decrease of cathode inlet relative humidity from 100% to 0 linearly in 0.25 seconds at $t=1$ sec.

The current responses undergo a sudden increase (about 5%) due to the relative effect of increasing oxygen inlet concentration as shown in Fig. 8. The slow decay that follows the initial jump is mainly due to that of membrane conductivity, which decreases due to decreasing water content of the membrane as shown in Fig. 7. Moreover, as the water content in the membrane decreases so does the water mass fraction in the cathode GDL. Thus, the oxygen mass fraction in the cathode GDL slowly increases after the initial jump, as shown in Fig. 8.

Not shown here, but responses to increasing cathode-inlet relative-humidity conditions are symmetric of what are shown here.

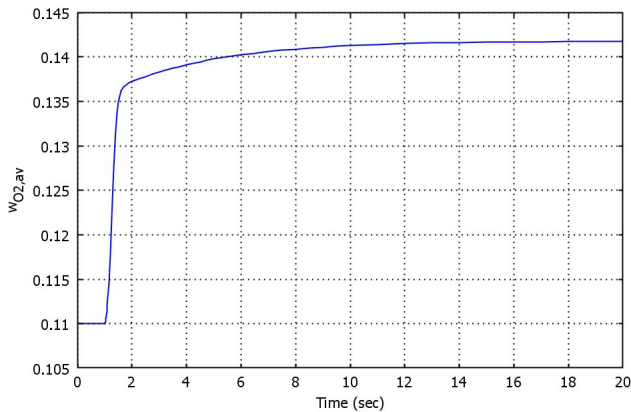


Fig. 8: Area averaged oxygen concentration at the membrane-cathode GDL interface with respect to time following the decrease of cathode inlet relative humidity from 100% to 0% linearly in 0.25 seconds at $t=1$ sec.

Cathode pressure drop transients

Pressures are specified for flows in cathode and anode flow channels at inlets and exits. In all simulations, anode pressure drop is kept the same, $\Delta p_a = 30$ Pa, and the cathode pressure drop is reduced from 500 Pa to 50 Pa at $t = 1$ s linearly with a ramp that lasts 0.25 s keeping the fuel cell voltage and the cathode-inlet relative-humidity constant, 0.75 Volts and zero respectively.

The average current drops following the transient of the pressure drop sharply first and remains nearly constant afterwards as depicted in Fig. 9 for different relative humidity conditions at the cathode inlet, and mass transfer coefficients. It is clear that cathode pressure drop can be used as a stable control mechanism for load variations at constant cell voltage.

Due to decreasing current density, electro-osmotic drag weakens and the membrane water concentration increases as shown in Fig. 10 varying slightly with respect to relative humidity at the cathode inlet. The effect of the humidification parameter is not significant in the current response in Fig. 9, but governs the response of the membrane water concentration.

CONCLUSIONS

A three-dimensional time-dependent model of a PEMFC section that contains a U-section of serpentine flow fields is introduced here. The isothermal model considers only gas phase water in the gas diffusion layers and the flow channels, and liquid water in the membrane. Neumann boundary conditions that incorporate a humidification parameter are used for the water concentration in the membrane.

The model is used to analyze transients of the electric load (as cell voltage), cathode-inlet relative-humidity, and cathode pressure drop. In load transients, average current always overshoots first, and then slowly decreases when the voltage is ramped from 0.75 to 0.7 Volts in a short time. The overshoot is due to decreased overpotential, and the slow decrease in the aftermath of the overshoot is due to the decrease in the cathode stoichiometric flow ratio, which varies since the pressure drop in the cathode gas channel is fixed at 500 Pa. Symmetric behavior is observed in our simulations, which are not shown here, when the voltage is increased. For the simulations conducted here, membrane water concentration plays a minor role in current responses to cell voltage transients, and the sensitivity with respect to the humidification parameter is not strong.

Observed transient time-scales are analyzed with a simple model, which is based on volume averaging of Eqs. (8), (26) and (27). It is shown that, for values of the humidification parameter used in simulations that are presented here, humidification time-scale is slower than the diffusive time-scale in the membrane. Hence the transients are governed by the humidification time-scale.

Humidification parameter, which governs the membrane water concentration, plays a major role in the cathode-inlet relative-humidity transients. In fact, current responses to relative-

humidity transients are mainly governed by the value of the humidification parameter.

Lastly, transients of the cathode pressure drop result in current responses that are simply governed by the stoichiometric flow ratio. As the pressure drop reduced cell-average current decreases at constant cell-voltage. Membrane water concentration undergoes through its typical decay transient, however its effect on the average cell current remains minor.

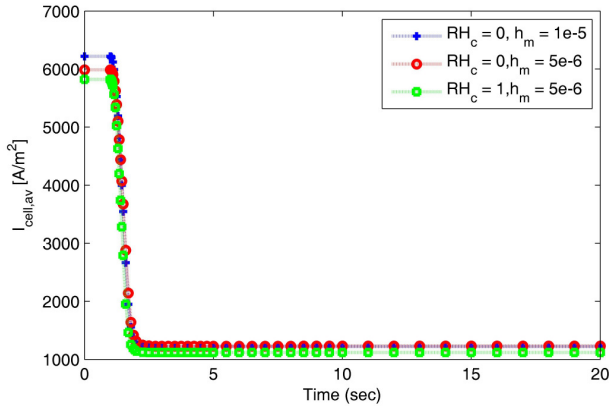


Fig. 9: Area averaged current density at the collectors with respect to time following the decrease of cathode pressure drop from 500 to 50 Pa linearly in 0.25 seconds at $t=1$ sec.

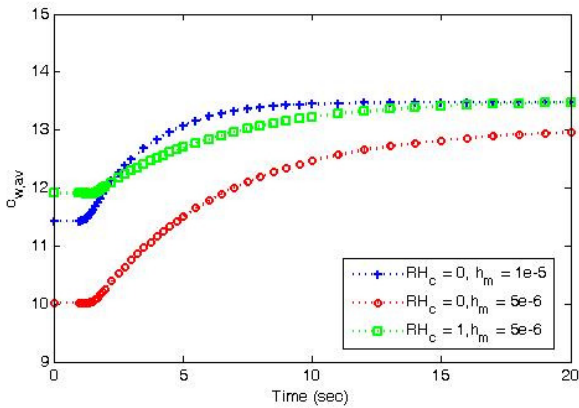


Fig. 10: Volume-averaged membrane-water concentration as a function of time following the decrease of cathode pressure drop from 500 to 50 Pa linearly in 0.25 seconds at $t=1$ sec.

ACKNOWLEDGMENTS

We kindly acknowledge the partial support for this work from The Scientific and Technological Research Council of Turkey (TUBITAK) under the contract number 104M136.

REFERENCES

- [1] Shimpalee, S. Spuckler, D. and Van Zee, J.W., 2007, "Prediction of transient response for a 25-cm² PEM fuel cell", *Journal of Power Sources*, **167**, 130-138.
- [2] Guilin, H., Jianren, F., 2007, "Transient computation fluid dynamics modeling of a single proton exchange membrane fuel cell with serpentine channel", *Journal of Power Sources*, **165**, 171-184.
- [3] Djilali, N., 2007, "Computational modeling of polymer electrolyte membrane (PEM) fuel cells: Challenges and opportunities", *Energy*, **32**, 269-280.
- [4] Springer, T.E., Zawodzinski, T.A., and Gottesfeld, S., 1991, "Polymer electrolyte fuel cell model", *J. Electrochem. Soc.*, **138**(8), 2334-2342.
- [5] Berg, P., Promislow, K. St. Pierre, J., Stumper, J. and Wetton, B., 2004, "Water management in PEM fuel cells", *J. Electrochem. Soc.*, **151**(3), A341-A353.
- [6] Baschuk, J.J. and Li, X., 2004, "A general formulation for a mathematical PEM fuel cell model", *Journal of Power Sources*, **142**, 134-153.
- [7] Okada, T., Xie, G., and Meeg, M., 1998, "Simulation for water management in membranes for polymer electrolyte fuel cells", *Electrochimica Acta*, **43**(14-15), 2141-2155.
- [8] Serincan, M.F., Yesilyurt, S., 2007, "Transient analysis of proton electrolyte membrane fuel cells (PEMFC) at start-up and failure", *Fuel Cells*, **7**(2), 118-127.
- [9] Chen, F., Su, Y-G., Soong, C-Y., Yan, W-M., Chu, H-S., 2004, "Transient behavior of water transport in the membrane of a PEM fuel cell", *J. Electroanalytical Chem.*, **566**, 85-93.
- [10] Bird, R.B., Stewart, W.E., Lightfoot, E.N., 2002, *Transport Phenomena*, 2nd ed, Wiley, New York.
- [11] Fuller, T.F., Newman, J., 1993, "Water and thermal management in solid-polymer-electrolyte fuel cells," *J. Electrochem. Soc.*, **140**, 1218-1225.
- [12] COMSOL, 2006, "COMSOL Multiphysics User Guide", COMSOL A.B., Stockholm.